Employing the Distribution of Interference to Improve Graph-Based Receiver

Abdullah A. Saed
Department of Communications Engineering
Faculty of Electronics Engineering
University of Mosul, Mosul, Iraq
abdcom_eng2006@yahoo.com

ABSTRACT: *In this paper, we investigate the influence of utilizing the distribution of multi-antenna interference (MAI) on the graph-based soft iterative receiver (GSIR) instead of applying the Gaussian approximation. It is shown Gaussian approximation is not only inaccurate at high signal-to-noise (SNR) ratio but also at low SNR with the availability of a priori information (during iterations). Consequently, it severely limits performance. It is demonstrated that implementing the distribution of interference at the data detection is able to double the bandwidth efficiency and improve the power efficiency dramatically. Even if the computational power is limited and a specific bandwidth efficiency is aimed, employing the distribution of interference can still achieve few dB gain with saving around 75 percentage of the available computational power compared to Gaussian approximation. Besides, a hybrid receiver that combines between employing the distribution of interference and applying the Gaussian approximation on interference is proposed. This combination is adjustable in the way that offers a real flexibility between performance and complexity. The performance characteristics of these kind of receivers are investigated via an Exit chart analysis. Additionally, Monte-Carlo simulation results showed that at BER = 10^{-3} the hybrid receiver needs only 1.9 dB to reach the performance of employing the distribution of interference with saving about 99.2 percentage of its computational power. The proposed method is applicable with any kind of GSIR with arbitrary modulation and channel coding schemes.*

Keywords: Graph-Based Receiver, Gaussian Approximation, GSIR, Signal-to-noise Ratio, Multi-antenna Interference

Received: 9 November 2012, Revised 22 December 2012, Accepted 24 December 2012

1. Introduction

The very high demand on the fast communication systems is explosively growing to satisfy the required advanced applications such as video calls. To improve the bandwidth efficiency, using higher-order modulation schemes is an indispensable solution. Where more than one information bits are mapped onto a single data symbol. In addition, implementing multiinput multi-output (MIMO) systems is another method to enhance the bandwidth efficiency and/or system performance. Therefore, utilizing higher-order modulations in MIMO systems has been proposed for emerging wireless radio systems such as 3GPP long term evolution (LTE).

To obtain a good system performance, accurate channel state information (CSI) is required. The receiver can estimate the CSI when known training symbols are embedded into the transmitted signal stream [1], [2]. In MIMO systems, the number of the required training symbols increases proportionally with the number of transmit antennas [3], which degrades the power and the bandwidth efficiency. Iterative receivers employing turbo principle that jointly implement data detection and channel estimation are a promising method to reduce the training symbols. Accordingly, they can efficiently refine the channel estimation by using the detected data symbols [4] – [6].

Graph-based soft iterative receivers (GSIR) have recently been proposed as a soft joint channel estimation and data detection [7] – [10]. The soft channel information is produced and refined during iterations for a MIMO system with BPSK over a block-fading channel in [7]. Utilizing a higher-order modulation for a SISO system over a time-varying channel has been presented in [9]. Furthermore, a 2-dimensional GSIR that works for MIMO-OFDM with BPSK over a time-varying frequency-selective channel has been proposed in [8]. Last but not least, a GSIR works for a MIMO-OFDM with arbitrarily modulation and channel coding schemes in multi-dimensional (e.g. time, frequency, and spatial domain) over a time-varying frequency-selective channel has been suggested in [10].

In all the proposed GSIRs, the MAI and the noise are approximated by a Gaussian variable. In other words, the residual interference's pdf, which represents convolving the pdfs of the interfering symbols with the noise pdf, is approximated by a Gaussian pdf. This assumption is accurate according to the central limit theorem as long as the number of the residual interferers is high [11]. However, the accuracy of this approximation reduces as much as the algorithm converges, since the reliability of the residual interferers increases that represents decreasing the variance of the interferers' pdf. This impact becomes more serious at high signal-to-noise ratio (SNR) than low SNR, as the interfering pdfs start with a smaller variances.

In a MIMO system, to obtain a good system performance, an efficient MAI cancellation is necessary. In the other hand, the efficiency of this cancellation strongly depends on the accuracy of the Gaussian approximation. With increasing SNR and when the algorithm converges the accuracy of the approximation reduces, which causes more residual error. The sensitivity to residual error increases with the modulation order, since the higher the modulation order is the smaller Euclidean distance has. Therefore, we propose to utilize the exact pdf of the residual interferers. The proposed GSIR can work with arbitrary modulation and channel coding schemes with any GSIR dimensions.

In this paper, the GSIR performance degradation caused by taking the Gaussian approximation on the MAI and the AWGN signal is investigated. In addition, considering the exact pdf of the residual interferers at the data detection stage is investigated for the case of perfect CSI and imperfect CSI. Since the reliability of the data detection and the channel estimation is mutual in the GSIR, implementing the exact pdf for the residual interferers at the data detection stage enhances the channel estimation reliability as well. Monte- Carlo simulations are provided to illustrate the performance gain for the proposed GSIR receiver. Besides, to have a compromise between performance and complexity, a hybrid GSIR is proposed.

The remainder of this paper is organized as follows: Section II defines the system and channel model, SM schemes, and the used GSIR. In Section III Gaussian approximation is explained, and the distribution of interferers is investigated as well as compared with the Gaussian approximation. Secection IV gives complexity comparison between the two methods. Then, the hybrid receiver is proposed in Section V. Numerical results are presented in Section VI and Section VII draws the conclusions.

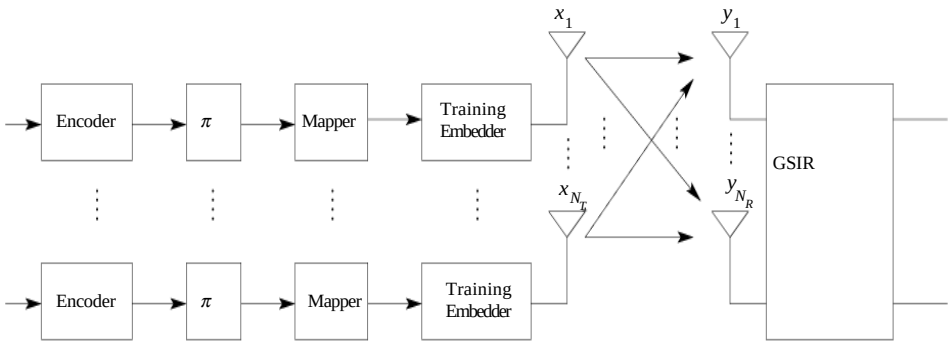

Figure 1. Bit-interleaved coded modulation with training insertion in a MIMO channel

2. Fundamentals

2.1 System and Channel Model

The considered system in this work is, a bit-interleaved coded transmission system [12] over a flat fading time-varying MIMO

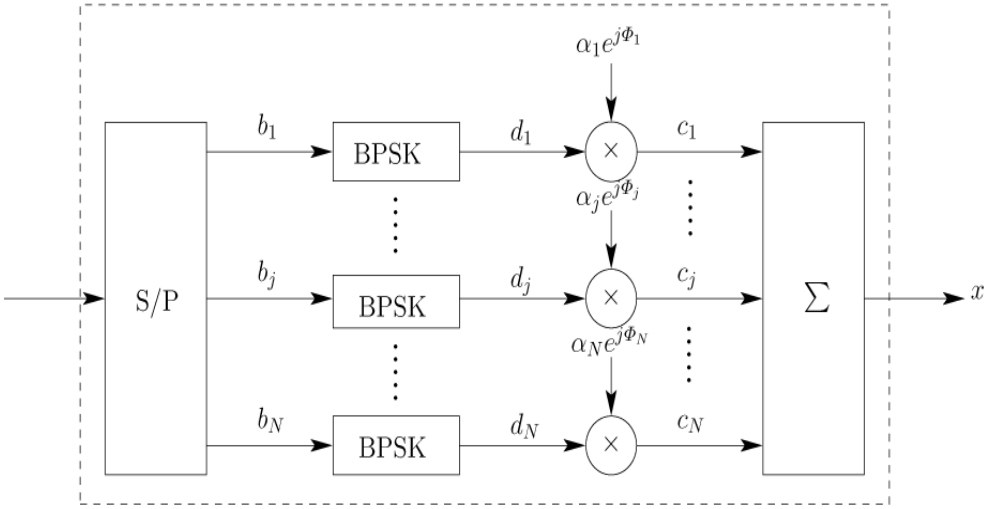

Figure 2. Superposition mapping (SM)

channel as shown in Figure 1. At the transmitter side, first the data symbols are encoded, then interleaved. Hence, the adjacent data symbols will be independent in time domain. Thereafter, the interleaved code bits are mapped and finally the pilot symbols are inserted among the data symbols along the burst. The received signal at the *n* receive antenna can be written as

$$y_n[k] = \sum_{m=1}^{N_T} h_{n,m}[k] \,.\, x_m[k] + w_n[k] \tag{1}$$

where N_R represents the number of the receive antennas, $k \in \{0, 1, ..., K-1\}$ is the discrete time index with K representing the burst length. $y_n[k] \in \mathcal{C}$ is the received signal (channel output) at the n-th ($1 \le n \le N_R$) *Rx* antenna at time index k, and $x_m[k]$ is the channel input at the m-th *Tx* antenna at time index k. $h_{n,m}[k] \in \mathcal{C}$ is the coefficient of the sub-channel connecting the n-th *Rx* antenna and the m-th *Tx* antenna at time index k. $w_n[k]$ denotes an AWGN sample with zero mean and variance σ_n^2. The channel is considered to be a wide-sense stationary uncorrelated scattering (WSSUS) channel model. Channel coefficients of each sub-channel can be emulated by a superposition of P paths as

$$h_{n,m}[k] = \lim_{P \to \infty} \frac{1}{\sqrt{P}} \sum_{p=1}^{P} \exp\left(\phi_p + 2\pi f_{D_p} T_s k\right) \tag{2}$$

where the p^{th} path has a randomly generated initial phase ϕ_p and a Doppler frequency of f_{D_p}. The symbol duration is represented by T_s [13].

2.2 Superposition Mapping

SM is a recently proposed mapping scheme that linearly superimposes a certain number of binary antipodal bits to produce a Gaussian like constellation signal [14]. Before summing up the binary antipodal bits, a specific magnitude and phase are allocated to each one as shown in Figure (2). Based on this assignment, more than one kind of SM is obtained. In order to describe the SM scheme mathematically, the following formula can be used [14].

$$x = \sum_{j=1}^{N} c_j = \sum_{j=1}^{N} d_j \,.\, \alpha_j \, e^{j\Phi_j}, \qquad d_j \in \{\pm 1\}, \tag{3}$$

where α_j is the allocated magnitude of the j^{th} bit, Φ_j is the assigned phase of the j^{th} bit.

SM has attracted a lot of attention, since its distribution satisfies the requirement to achieve the channel capacity of the AWGN channel according to Shannon information theory [17]. In this paper, phase-shifted superposition mapping (PSM) is selected for its nearly Gaussian distributed constellation diagram as shown in Figure 3 and Figure 4, which supports the applied Gaussian approximation on the MAI and AWGN. More details about PSM is available in [14] – [16].

2.3 Factor Graph Model

Factor graphs are an efficient tool for designing iterative estimation / detection algorithms [18] – [19].

Without loss of the generality, the factor graph for coded transmission over a time-varying MIMO flat fading channel with $N_T = N_R = 2$ and $N = 2$ is illustrated in Figure 5. The channel nodes h that carry the information of the channel coefficients and the bit nodes $d_{m,j}$ that carry the information of the code bits are plotted in circles. While, the observation nodes y carry the information of the received symbols are plotted in rectangles. Two types of observations nodes are available. The first is the training observation nodes which are associated with the training symbols, while the others represent the data observation nodes. Meanwhile, the boxed plus represents a code node. For time-varying channel transition nodes are introduced that are denoted by a boxed Δ, which stand for the relationship between a channel node $h_{n,m}[k \pm 1]$ and its neighboring channel nodes $h_{n,m}[k]$. Moreover, information exchange between neighboring channel nodes is done throughout transition nodes. The channel nodes h carry the estimated soft CSI. The observation nodes y carry the received information as well as they are responsible for computing the log-likelihood ratio (LLR) values for each code bit and refining the estimated soft CSI at the data observation nodes. The $d_{m,j}$ contains the LLR for the j^{th} code bit.

To simplify how the GSIR works, a step by step explanation is given below:

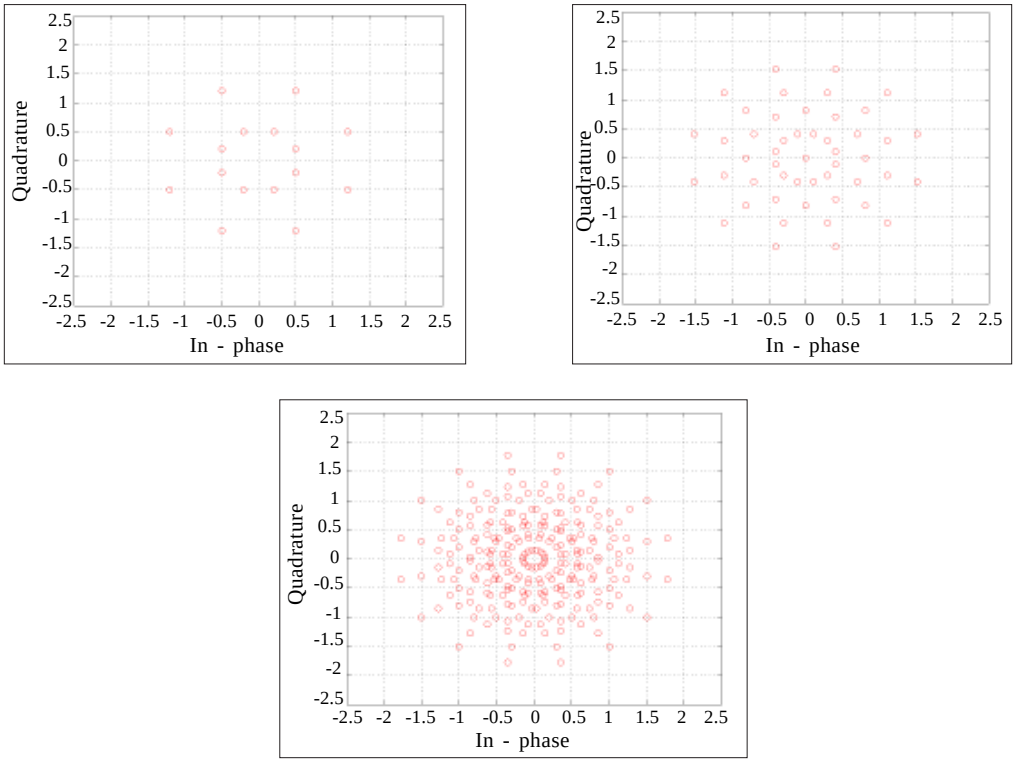

Figure 3. Constellation diagram for PSM with $N = 4$, 6 and 8 respectively

As soon as the whole burst is received, the algorithm starts working as follows:

1) At first, soft channel estimate is performed at the training observation nodes, where the estimate value is [7]

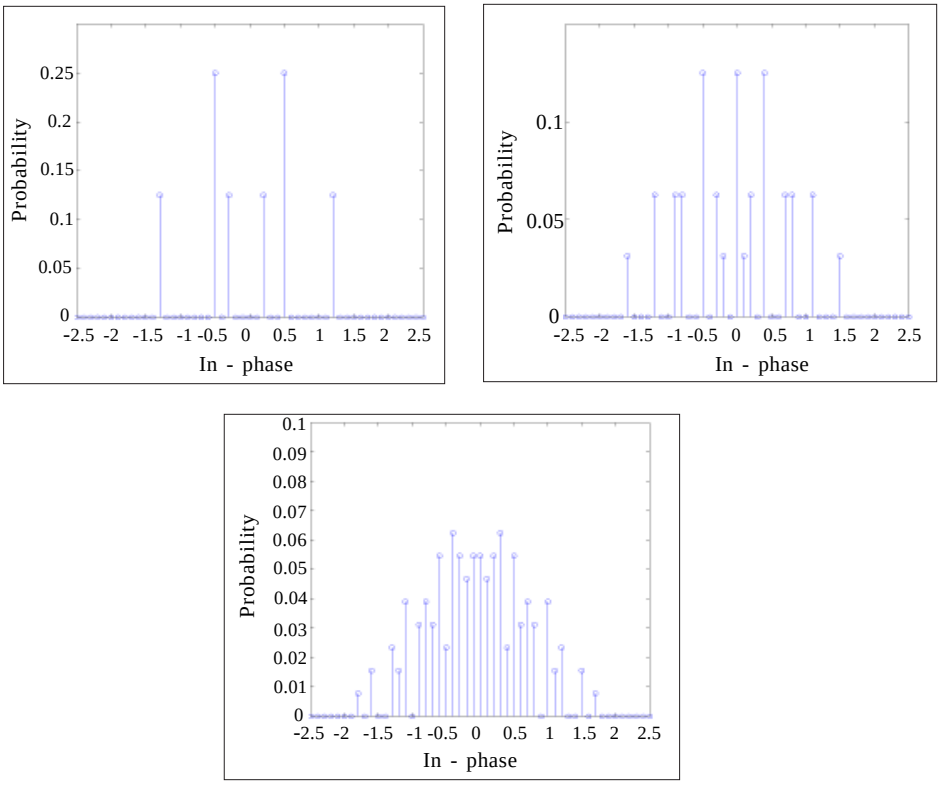

Figure 4. Distribution of Refxg for PSM with N = 4, 6 and 8 respectively

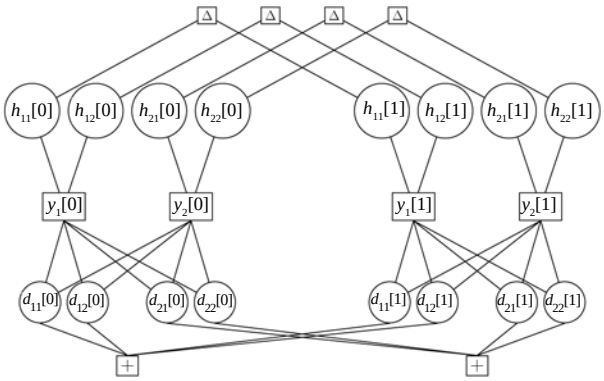

Figure 5. GSIR for a time-varying MIMO channel with $N_T = N_R = 2$ and $N = 2$

$$\mu_h = \frac{y}{x} \tag{4}$$

and the uncertainty of this estimate is

$$\sigma_h^2 = \frac{\sigma_w^2}{|x|^2} \tag{5}$$

Thus, soft CSI is represented by

$$h \sim \mathcal{CN}(\mu_h, \sigma_h^2) \tag{6}$$

This soft CSI is passed to the associated channel nodes.

2) The soft CSI is spread over the whole burst by means of forward and backward propagation. μ_h is passed without change to the neighboring channel nodes. While, σ_h^2 is increased by the variance of the transition node in each passing. The variance of

the transition nodes is obtained [8] as follows:

$$\sigma_{\Delta}^{2} = 2 - 2\,J_{o}(2\pi\, f_{D,max} T_{s}) \tag{7}$$

After distributing the soft CSI information along the burst, each channel node obtains its soft CSI by implementing the sum-product algorithm and forwards it to the associated data observation nodes.

3) The LLR for each code bit is calculated at the data observation nodes as follows:

$$LLR\,(d_{n,s}) = \log \frac{p\,(y \mid d_{n,s} = +1)}{p\,(y \mid d_{n,s} = -1)} \tag{8}$$

Before, the likelihood function for each hypothesis is calculated after eliminating the influence of the MAI and AWGN signals from the received signal as follows [9]:

$$p\,(y \mid x) = \frac{1}{\pi(\sigma_{h}^{2} \mid x \mid^{2} + \sigma_{v}^{2})} \exp\left(-\frac{\mid (y - \mu_{v}) - \mu_{h} x \mid^{2}}{\sigma_{h}^{2} \mid x \mid^{2} + \sigma_{v}^{2}}\right) \tag{9}$$

where μ_{v} and σ_{v}^{2} represent the mean and variance of the interfering Gaussian variable (MAI + AWGN) respectively, which will be explained in details in Section III-A. Then, LLRs are passed to their associated bit nodes. Since more than one receive antenna is employed, each bit node receives LLRs by the number of N_{R}. The received LLRs at each bit node are summed up to get the spatial diversity gain before been sent to its related code node.

4) Code nodes generate extrinsic information and pass them to their connected bit nodes, which calculate the a priori information for each code bit $P_{d,\pm 1}$ before passing them to their associated data observation nodes. This step declares the beginning of iterations.

5) Data observation nodes calculate the a priori information for each symbol hypothesis P_{x} to be used for calculating the channel coefficients as follows [9]:

$$\mu_{h} = \gamma\,(y - \mu_{v}) \sum_{x \in \chi} P\,(x) / (x \mid x \mid^{2})$$

$$\sigma_{h}^{2} = \gamma\,(\sigma_{v}^{2} + \mid y \mid^{2}) \sum_{x \in \chi} P\,(x) / \mid x \mid^{4} - \mid \mu_{h} \mid^{2} \tag{10}$$

where

$$\gamma = \frac{1}{\sum_{x \in \chi} P\,(x) / \mid x \mid^{2}} \tag{11}$$

and pass them to their connected channel nodes. Besides, training observation nodes perform soft channel estimate as described in step 1.

6) Each channel node exchanges its messages with its neighboring channel nodes. Then, they refine their messages by mean of sum-product algorithm before passing them to their associated data observation nodes.

7) With the presence of the refined soft CSI and the a priori information, each data observation node performs soft data detection as already described in step 3.

Iterations go on until a specific condition is met. During iterations, it is expected the reliability of the a priori information is enhanced, which improves the performance of the data detection and the channel estimation. More details about GSIR is available in [7] – [10].

3. MAI Cancellation

3.1 Gaussian Approximation

Gaussian approximation is known from the multiuser systems. It has been used in multiple-access/multiplexing systems [20]. The idea of this approximation in short words is to approximate the interfering code bits and the AWGN sample by a Gaussian variable $v_{n,m,s} \sim \mathcal{CN}(\mu_h, \sigma_h^2)$. Its mean and variance are calculated to be utilized for MAI cancellation at the soft data detection and soft channel estimation. In [7], the Gaussian approximation that considers the reliability of channel estimate for BPSK has been derived. In the following, it will be derived for arbitrary higher-order mapping schemes.

For simplicity the time index *k* is omitted. After re-writing Equation (1), we get

$$y_n = x_s . h_{n,s} + \underbrace{\sum_{m=1,\, m \neq s}^{N_T} h_{n,m} . x_m}_{\text{MAI}} + \underbrace{w_n}_{\text{AWGN}} \tag{12}$$

The MAI and AWGN are approximated by a Gaussian variable $v_n \sim \mathcal{CN}(\mu_{v_n}, \sigma_{v_n}^2)$.

When bijective mapping schemes are utilized, calculating the mean and variance of v_s is performed symbol-wisely. Hence, the complexity grows exponentially with *N*. To get the statistics of the effective interfering sample, we define

$$\Gamma_m = x_m . h_m \tag{13}$$

therefore

$$\mu_{\Gamma_m} = \mu_{x_m} . \mu_{h_m}$$

$$\sigma_{\Gamma_m}^2 = E\{|\Gamma_m|^2\} - |\mu_{\Gamma_m}|^2$$

The mean and the variance of the Gaussian variable v_n are calculated as follows:

$$\mu_{v_n} = \underbrace{\sum_{m=1,\, m \neq s}^{N_t} \mu_{\Gamma_m}}_{\text{MAI}}$$

$$\sigma_{v_n}^2 = \underbrace{\sum_{m=1,\, m \neq s}^{N_T} \sigma_{\Gamma_m}^2}_{\text{MAI}} + \underbrace{\sigma_w^2}_{\text{AWGN}} \tag{14}$$

After some mathematical derivations, μ_{Γ_m} and $\sigma_{\Gamma_m}^2$ can be calculated according to

$$\mu_{\Gamma_m} = \mu_h . \sum_{r=1}^{R} x_r . P(x_r)$$

$$\sigma_{\Gamma_m}^2 = |\mu_h|^2 . \sum_{r=1}^{R} |x_r|^2 . P(x_r) - |\sum_{r=1}^{R} x_r . P(x_r)|^2 \tag{15}$$

where $R = 2^N$, which shows how the computational complexity grows exponentially with *N* and linearly N_t.

MIMO system performance is sensitive to the accuracy of MAI cancellation. Consequently, it is directly affected by the accuracy of Gaussian approximation particularly when higher-order mapping schemes are utilized. Therefore, it is worthwhile investigating it.

The accuracy of Gaussian approximation depends on two parts. First, number of interferers. To increase number of interferers, higher-order mapping schemes are selected and/or more transmit antennas are employed. In the one hand, that also supports the

bandwidth efficiency, which is absolutely demanded, but on the other hand increasing the modulation order increases the sensitivity to residual errors, which unfortunately degrades the system performance. Adding more transmit antennas requires more signal overhead that again degrades the bandwidth and power efficiency. Second, uncertainty of interferers, which is inversely proportional to SNRs. Besides, it also decreases with the system convergence (during iterations).

2.2 Exact pdf of MAI and AWGN

To the best knowledge of the author, in all the published works [7] – [10] when GSIR is implemented in MIMO, Gaussian approximation has been applied for MAI and AWGN sample. In this Sec. the exact pdf of interferers will be investigated and compared with the Gaussian approximation.

For the sake of simplicity y_n is denoted as y in the following. As it is clearly seen in Equation (12), the received signal consists of the interesting term $x_s \,.\, h_s$, MAI, and noise. The last two terms are considered the interfering part that are described as:

$$I_{x_s} = \underbrace{\sum_{m=1,\, m \neq s}^{N_T} h_m \,.\, x_m}_{\text{MAI}} + \underbrace{w}_{\text{AWGN}} \tag{16}$$

The pdf of I_{x_s} is the convolution of the $(N_T - 1)$ pdfs of the MAI and the normal pdf as follows:

$$f_{I_{x=1}} = (f_{x=2} \,.\, h_2) * (f_{x=3} \,.\, h_3) * \ldots * (f_{x=N_T} \,.\, h_{N_T}) * \frac{1}{2\pi\sigma_w^2} e^{-\frac{|z|^2}{2\sigma_w^2}} \tag{17}$$

The pdf of each transmitted symbol f_x is obtained according to the following formula:

$$f_x = \sum_{i=1}^{R} P(x_i)\, \delta(z - x_i) \tag{18}$$

where δ is the Dirac pulse in the complex plane and $P(x_i)$ is the probability of symbol, which is already calculated at the data

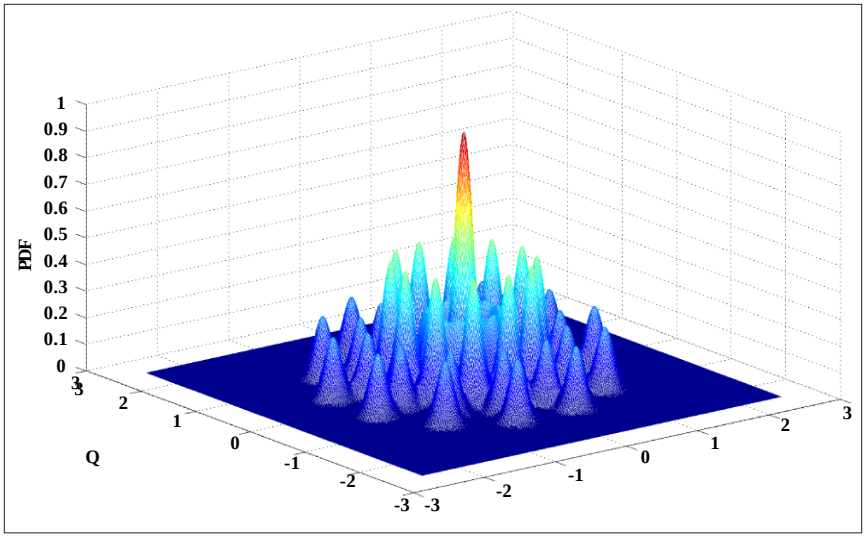

Figure 6. Exact pdf of MAI, and noise for MIMO $2 * 2$, $N = 6$, perfect CSI, $h = 1$, no a priori information, and $Eb/N_o = 15dB$

observation nodes during iterations.

As it is obvious in Equation (18), f_x consists of pulses that are located at the symbol values on the complex plane. After multiplying the pdf of each interfering symbol by its channel coefficient as given in Equation (17), their locations are shifted to $x_i \,.\, h$.

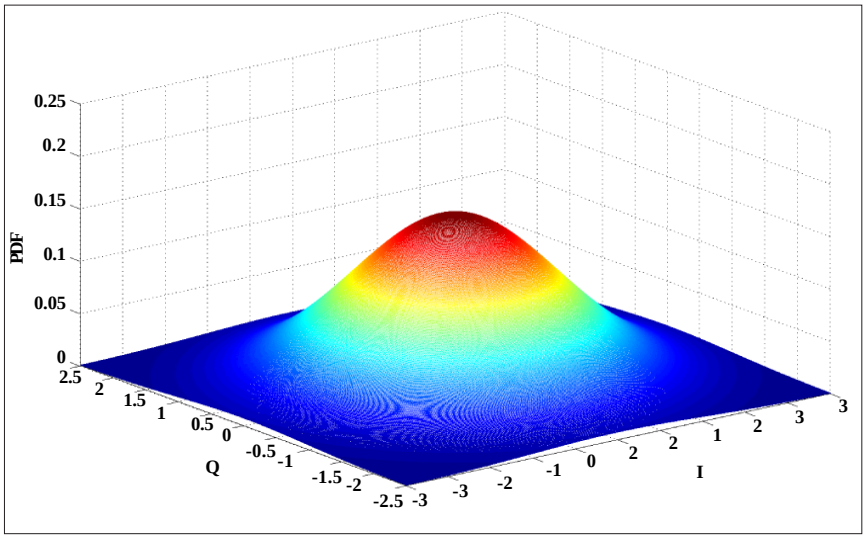

Figure 7. Pdf of MAI, and noise with Gaussian assumption for MIMO $2 * 2$, $N = 6$, perfect CSI, $h = 1$, no a priori information, and $Eb/N_o = 15dB$

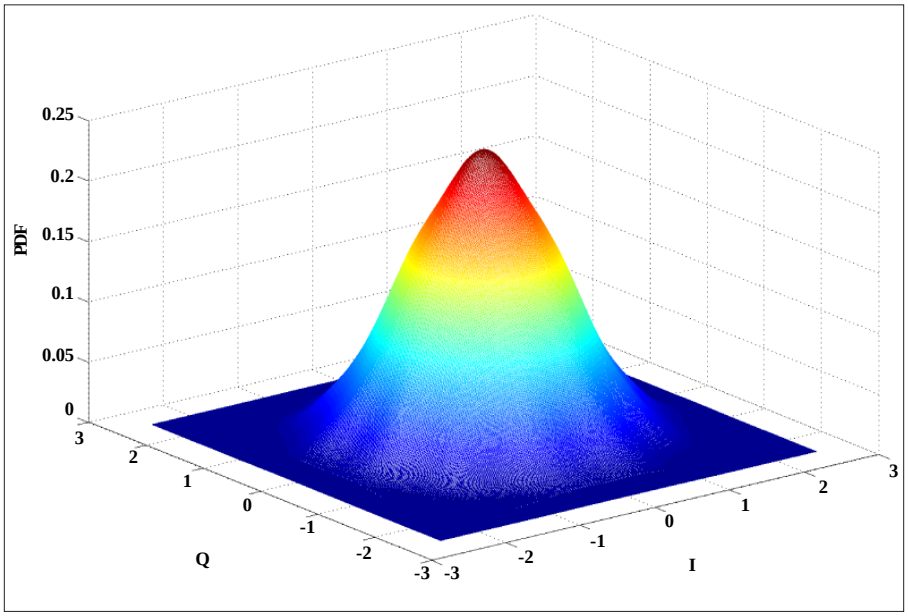

Figure 8. Exact pdf of MAI, and noise for MIMO $2 * 2$, $N = 6$, perfect CSI, $h = 1$, no a priori information, and $Eb / N_o = 5dB$

Convolving two discrete pdfs in the complex plane can be calculated as

$$f_{x1} * f_{x2} = \sum_{i=1}^{R} \sum_{j=1}^{R} P(x_{1_i}) P(x_{2_i}) \delta(z - (x_{1_i} + x_{2_i})) \tag{19}$$

2.3 Comparison of the Exact pdf with Gaussian Approximated pdf

To imagine the difference between the exact pdf and the Gaussian approximated pdf, some graphs will be given in the following. We assume MIMO with $N_T = N_R = 2$, $N = 6$, no a priori information is available, and perfect CSI with $h = 1$.

Figure 6 shows the exact pdf of the interference. Meanwhile, Figure 7 gives the pdf of the interference using the Gaussian approximation. For both pdfs $10\log \frac{Eb}{N_o} = 15\ dB$. *Eb* is the average bit energy and N_o denotes the single-sided power spectral density of the Gaussian noise. Clearly, the Gaussian approximated pdf is much different from the exact pdf, although they have the same mean and variance. However, as already mentioned, at low SNRs the Gaussian approximated pdf gets closer to the exact pdf as shown in Figure 8 and Figure 9 for SNR = 5 dB.

Unfortunately, even this rough similarity at low SNRs is broken as the reliability of the interfering symbols increases during iterations as shown in Fig. 10.

4. Complexity Comparison

To perform soft data detection as described in step 3 of Section II-C, which approximates the (MAI + AWGN) by a Gaussian variable, it is required to go through $2N_T\ 2^N$ constellation points. However, it needs to visit $2^{N \cdot N_T}$ points for the case of calculating the exact pdf of interferers.

5. Hybrid Receiver

So far, it is concluded that Gaussian approximation has simple complexity that is practically needed. But, this interesting property is priced with performance degradation either at high SNRs or at low SNRs with availability of reliable a priori information. In the other hand, employing the exact pdf significantly improves the performance. Regretfully, such gain is not earned for free, it requires complicated computations. Hence, it is worthwhile investigating a receiver that compromises in between.

The main complexity difference between the two methods grows exponentially with N_T for the case of the exact pdf and linearly for the other case. This difference becomes prohibitive with high N_T particularly when high *N* is selected, because all the pdfs of the interfering symbols are considered in the convolution.

To have a compromise between performance and complexity, we propose a hybrid receiver that calculates the exact pdf for a part of the interfering symbols and considers the Gaussian approximation for the remaining part. In this way, its complexity growth and performance improvement in contrast to implementing the Gaussian approximation depend on how many interfering symbols are considered for the exact pdf.

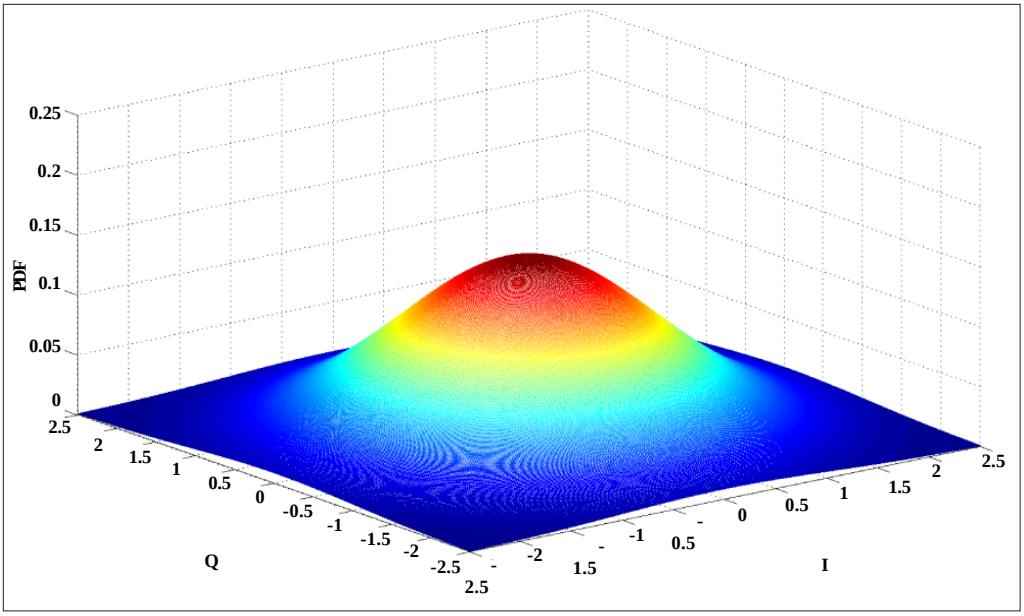

Figure 9. Pdf of MAI, and noise with Gaussian assumption for MIMO $2 * 2$, $N = 6$, perfect CSI, $h = 1$, no a priori information, and $Eb / N_o = 5$dB

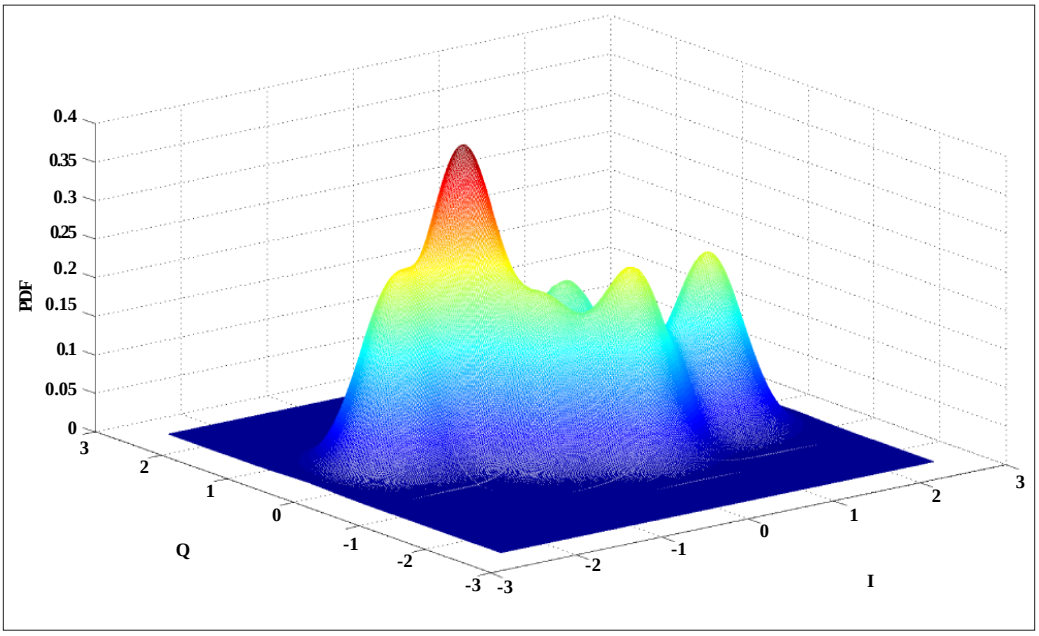

Figure 10. Exact pdf of MAI, and noise for MIMO $2 * 2$, $N = 6$, perfect CSI, $h = 1$, with a priori information availability, and $Eb / N_o = 5$dB

In the proposed receiver, the mean μ_u and variance σ_u^2 of the interfering symbols, which are approximated by a Gaussian variable, and the AWGN are calculated at first according to Equation (14), before convolving them with the pdfs of the remaining interfering symbols that are considered for the exact pdf calculation as follows:

$$f_{I_x} = (f_{x=1} .\ h_1) * (f_{x=2} .\ h_2) *...* (f_{x=q} .\ h_q) * \frac{1}{\pi \sigma_u^2} e^{-\frac{|z-\mu_u|^2}{\sigma_u^2}} \tag{20}$$

where q is the number of pdfs that are selected to consider their exact pdf. The trade off between performance and complexity can

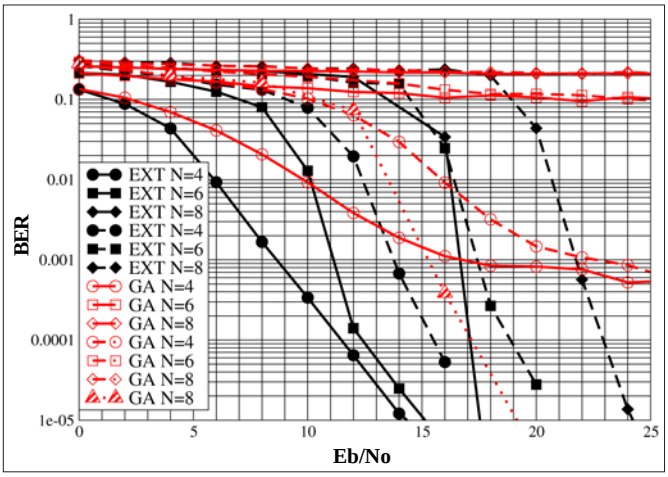

Figure 11. BER comparison between the exact pdf and the GA pdf in MIMO $2 * 2$ with a code rate of $\frac{1}{2}$ for all curves except the plotted curve with triangle, where its code rate is $\frac{1}{4}$. Solid lines stand for perfect CSI and dashed lines denote the imperfect CSI

be executed by adapting q. If $q = N_T - 1$ is chosen, the performance of the receiver employing the exact pdf can be obtained. Meanwhile, reducing q relaxes the complexity and degrades the performance compared to the case of the exact pdf till $q = 0$ the

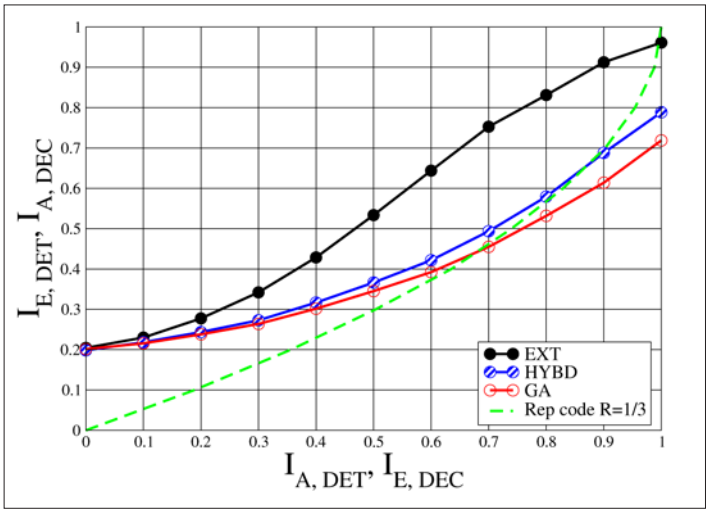

Figure 12. EXIT chart analysis of the exact pdf, hybrid pdf (with q =1), and GA pdf, Eb/N_o = 12dB, N_T = 4, N_R = 2, and N = 4

performance of implementing the Gaussian approximation is reached. Besides, q can even be adjusted during iterations to allow more flexibility.

6. Simulation Results

In this section, a comparison of the bit error rate (BER) performance for the GSIR when the exact pdf of interferers is considered (EXT pdf), the Gaussian approximated pdf of interferers is applied (GA pdf), and for the hybrid pdf of interferers is taken into account (HYBD pdf). PSM scheme and repetition code are chosen. Number of iterations is selected to be 10. The data symbols are transmitted through a Rayleigh fading channel with a normalized maximum Doppler frequency $f_D T_s$ = .005. The training symbol spacing D_T = 8 is used.

At first, the BER performance of the GSIR employing the exact pdf and the GA pdf depending on N is compared in Figure 11. N_T = N_R = 2 with a code rate $\frac{1}{2}$ are selected. For N = 4 with perfect CSI, the GA pdf suffers from severe error floor at BER = 5. 10^{-4}. However, at the same BER, the exact pdf offers 14.5 dB gain and it even reaches BER=105 at SNR=14.3 dB. Although increasing N is supposed to enhance the GA pdf, it adversely affects on its performance as shown in Figure 11. This is interpreted as enlarging N reduces the Euclidean distances, which makes it more sensitive to residual error created by the inaccuracy of Gaussian approximation. Nevertheless, the exact pdf can properly work with high N such as 6, and 8 for both perfect and imperfect CSI.

Regarding the bandwidth efficiency, The GA pdf can achieve 4 bit/sec/Hz, but with severe error floor. Meanwhile, the exact pdf can properly support till 8 bit/sec/Hz with much better power efficiency. But on the other hand, the required complexity for the exact pdf is higher than the needed complexity for the GA pdf. To make a fair comparison, the bandwidth efficiency for both methods will be compared in the same environment and let them consume roughly the same computational complexity. For the GA pdf, the code rate $\frac{1}{4}$ and N = 8 are compared with exact pdf for the N = 4 and code rate $\frac{1}{2}$ in Figure 11. Clearly seen that the exact pdf achieves around 1.5 dB gain at BER=104, even though it needs to go through only 2^8 constellation points and the GA pdf visits 2^{10} points. Concerning making another fair comparison to achieve a higher bandwidth efficiency than 4 bit/sec/Hz, the GA pdf can not succeed even with a very low code rate.

In the second scenario, the hybrid pdf (with q = 1) is considered for comparison as well, where N_T = 4, N_R = 2, and N = 4 are selected. To have an insight about the performance of the three methods, they are first examined by the extrinsic information transfer (EXIT) chart analysis [21], [22], which represents an efficient tool to study the convergence performance of iterative receivers.

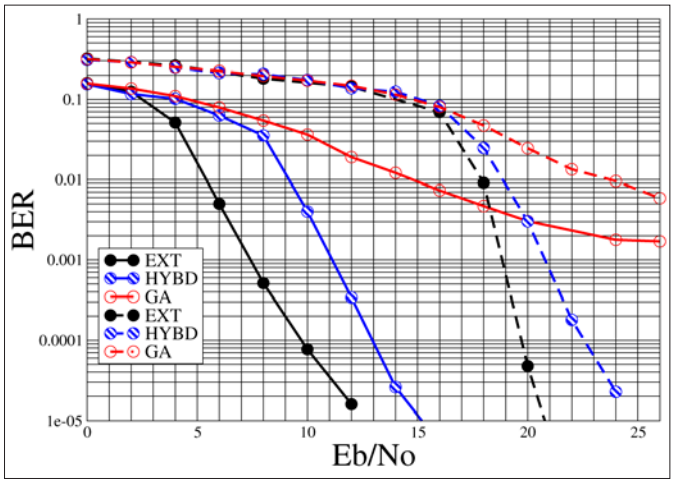

Figure 13. BER comparison for the exact pdf, GA pdf, and the hybrid pdf (with $q = 1$) in MIMO $4 * 2$ with a code rate of $\frac{1}{3}$. Solid lines stand for perfect CSI and dashed lines denote the imperfect CSI.

Figure 12 illustrates the transfer function of the three methods for an SNR of 12dB assuming perfect CSI. It is shown that they start at the same point. Meanwhile, with increasing the reliability of the a priori information, the performance difference reveals. However, in conjunction with repetition code of rate $\frac{1}{3}$, the GA pdf intersects with it early at $I_{A_{DEC}} = 0.44$, which indicates a severe error floor regardless number of interations. On the contrary, the hybrid pdf can delay the intersection with the channel code to achieve $I_{A_{DEC}} = 0.65$, which offers a considerable gain. In the other hand, the exact pdf dramatically outperforms the others. Because of its very wide tunnel, it can achieve a very low BER with a low number of iterations that is highly demanded to reduce computational complexity.

To confirm the results of the EXIT chart analysis, the BER performance of the three methods in the same scenario is given in Figure 13. At BER = $2 . 10^{-3}$, the exact pdf outperforms the hybrid pdf about 3.8 dB for the perfect CSI and about 1.8 dB for the imperfect CSI. While, the hybrid pdf achieves around 12.4 dB gain for the perfect CSI at BER = $2 .10^{-3}$. In the hybrid pdf even though q is chosen to be 1, which considerably reduces the computational complexity compared to the exact pdf, it achieves much better performance than the GA's performance and a little worse performance than the exact pdf's performance. To imagine the complexity difference of this scenario, the exact pdf goes through 2^{16} constellation points, while the hybrid pdf visits around 2^9 points, Meanwhile, the GA pdf considers 2^7 constellation points.

7. Conclusion

The effect of employing the distribution of interference on the GSIR performance has been spotlighted in this paper. It was shown that Gaussian approximation is not accurate at high SNRs and even at low SNRs with the presence of a priori information. Simulation results clearly demonstrated how utilizing the distribution of interference at the data detector can dramatically improve the bandwidth and power efficiency. Moreover, with a specific bandwidth efficiency, it can offer better performance and save considerable complexity compared to the Gaussian approximation. Additionally, a hybrid receiver that compounds between the two methods was proposed. This receiver flexibly compromises between performance and complexity. Simulation results showed not only does it offer an impressive gain, but also does it reduce complexity dramatically. These results are also verified by the EXIT chart analysis.

Finally, it is worth pointing out when N_T and N are not large (ex: $N_T = 2$, $N = 4, 6$), employing the distribution of interference is recommended. Meanwhile, for higher values the hybrid receiver is advised.

As a matter of fact, this work can straightforwardly be applied with any GSIR dimensions regardless of the modulation and

channel coding schemes. For extra performance improvement, it is worthwhile investigating how to consider the distribution of interference in the channel estimation as well.

References

[1] Cavers, J. K. (1991). An analysis of pilot symbol assisted modulation for Rayleigh fading channels, *IEEE Trans. Veh. Technol.*, 40 (4) 686–693, Nov.

[2] Lo, N. W. K., Falconer, D. D., Sheikh, A. U. H. (1991). Adaptive equalization and diversity combining for mobile radio using interpolated channel estimates, *IEEE Trans. Veh. Technol.*, 40 (3) 636–645, Aug.

[3] Hassibi, B., Hochwald, B. M. (2003). How much training is needed in multiple-antenna wireless links? *IEEE Trans. Inf. Theory*, 49 (4) 951–963, Apr.

[4] Valenti, M. C., Woerner, B. D. (2001). Iterative channel estimation and decoding of pilot symbol assisted turbo codes over flat-fading channels, *IEEE J. Sel. Areas Commun.*, 19 (9) 1697–1705, Sep.

[5] Sanzi, F., Jelting, S., Speidel, J. (2003). A comparative study of iterative channel estimator for mobile OFDM systems, *IEEE Trans. Wireless Commun.*, 5 (2) 849–859, Sep.

[6] Cozzo, C., Hughes, B. (2003). Joint channel estimation and data detection in space-time communications, *IEEE Trans. Commun.*, 51 (8) 1266–1270, Aug.

[7] Wo, T., Liu, C., Hoeher, P. A. (2008). Graph-based iterative Gaussian detection with soft channel estimaton for MIMO systems, *In:* Proc. 7th International ITG Conference on Source and channel Coding (SCC 2008), Ulm, Germany, Jan.

[8] Knievel, C., Shi, Z., Hoeher, P. A., Auer, G. (2010). 2D graph-based soft channel estimaton for MIMO-OFDM, *In:* Proc. IEEE International Conference on Communications, Capetown, South Africa, May.

[9] Shi, Z., Wo, T., Hoeher, P. A., Auer, G. (2010). Graph-based soft iterative receiver for higher-order modulation, *In:* Proc.12th IEEE International Conference on Communication and Technology (IEEE ICCT 2010), Nanjing, China, Nov.

[10] Knievel, C., Hoeher, P. A., Tyrrell, A., Auer, G. (2012). Multi-dimensional graph-based soft iterative receiver for MIMO-OFDM, *IEEE Transaction on Communications*, 60 (6) 1599–1906, June.

[11] Proakis, J. (1995). Digital Communications, McGraw–Hill, New York, NY, USA, 3rd edition.

[12] Caire, G., Taricco, G., Biglieri, E. (1998). Bit-interleaved coded modulation, *IEEE Trans. Inf. Theory*, 44 (3) 927–946, May.

[13] PHoeher, P. A. (1992). A statistical discrete-time model for the WSSUS multipath channel, *IEEE Trans. Veh. Technol.*, 41 (4) 461–468, Nov.

[14] Wo, T., Hoeher, P. A. (2010). Superposition mapping with application in bit-interleaved coded modulation, *In*: Proc. 8th International ITC Conference on Source and channel Coding (SCC '10), Siegen, Germany, Jan.

[15] Wo, T., Noemm, M., Hao, D., Hoeher, P. A. (2010). Iterative processing for superposition mapping, *Journal of Electrical and Computer Engineering*, v. 2010 p.13.

[16] Noemm, M., Wo, T., Hoeher, P. A. (2010). Multilayer APP detection for IDM, *Electronics Letters*, 46 (1) 96–97, Jan.

[17] Cover, T. M., Thomas. Elements of Information Theory, 2nd Edition. Johan Wiley & Sons, Ins.

[18] Kschischang, F. R., Frey, B. J., Loeliger, H.-A. (2001). Factor graphs and the sum-product algorithm, *IEEE Trans. Inform. Theory*, 47 (2) 498–519, Feb.

[19] Loeliger, H.-A., Dauwels, J., Hu, J., Korl, S., Ping, L., Kschischang, F. R. (2007). The factor graph approach to model-based signal processing, *In*: Proc. *IEEE*, 95 (6) 1295–1322, June.

[20] Schoeneich, H., Hoeher, P. A. (2003). A hybrid multiple access scheme approaching single user performance, *In*: Proc. Sixth Baiona Workshop on Signal Processing in Communications, Baiona, Spain, Sept, p. 163–168.

[21] Ten Brink, S. (2001). Convergence behavior of iteratively decoded parallel concatenated codes, *IEEE Trans. Commun.*, 49, p. 1727–1737, Oct.

[22] Ten Brink, S., Kramer, G., Ashikhmin, A. (2004). Design of low-density parity-check codes for modulation and detection, *IEEE Trans. Commun.*, 52 (4) 670–678, Apr.